Additively Manufactured High Power Microwave Anodes

Nicholas M. Jordan, *Member, IEEE*, Geoffrey B. Greening, *Student Member, IEEE*, Brad W. Hoff, *Member, IEEE*, Sabrina S. Maestas, Steven C. Exelby, *Student Member, IEEE*, and Ronald M. Gilgenbach, *Life Fellow, IEEE*

***Abstract*— Additively manufactured components were successfully fielded for the first time in a relativistic crossed-field device. Anode structures for a relativistic planar magnetron were 3-D printed from a photopolymer using a stereolithography printing process. One anode was electroplated with copper (RPM-12b), whereas the other was thermal sprayed with copper (RPM-12c). The coating thicknesses at the vane tips were approximately 0.18 and 0.23 mm, respectively. The performance and durability of these structures were evaluated in comparison with a solid aluminum anode (RPM-12a) fabricated via conventional machining. The experimental parameters were cathode voltages between −150 and −300 kV, voltage pulse lengths of 200 to 600 ns, axial magnetic fields of 0.13 to 0.31 T, peak anode currents from 1 to 7 kA, and a base operating pressure of 9×10^{-6} torr. The 3-D printed anodes demonstrated microwave performance comparable to the aluminum anode, generating microwave powers in excess of 150 MW, with an average instantaneous peak total efficiency of 27% ± 10%. After 100 shots on each structure, neither anode showed any signs of operationally induced damage. The anodes did, however, have a higher rate of postshot outgassing, emitting 32% and 23% more CO_2 per shot, respectively.**

***Index Terms*— 3-D printing, additive manufacturing, anodes, metallization, microwave devices, plastics.**

I. Introduction

HIGH-POWER microwave sources serve a number of important applications in defense, industrial, and scientific fields. These applications include radar, materials processing, and counter electronics [1]–[3]. For some applications, source mobility is desirable. Unfortunately, many high-power microwave sources can be massive enough that incorporating these devices into mobile platforms becomes problematic. Replacing source components with equivalently functional less massive counterparts is one way to address issues with overall system weight.

Manuscript received January 15, 2016; revised March 17, 2016; accepted April 24, 2016. Date of publication May 26, 2016; date of current version August 9, 2016. This work was supported in part by the Directed Energy Professional Society, in part by L-3 Communications Electron Devices, and in part by the Air Force Office of Scientific Research under Grant FA9550-15-1-0097.

N. M. Jordan, G. B. Greening, S. C. Exelby, and R. M. Gilgenbach are with the University of Michigan, Ann Arbor, MI 48019 USA (e-mail: jordann@umich.edu; geofgree@umich.edu; scexlb@umich.edu; rongilg@umich.edu).

B. W. Hoff and S. S. Maestas are with the Air Force Research Laboratory, Kirtlan AFB, NM 87117 USA (e-mail: brad.hoff@us.af.mil; sabrina.maestas@us.af.mil).

Color versions of one or more of the figures in this paper are available online at http://ieeexplore.ieee.org.

Digital Object Identifier 10.1109/TPS.2016.2565261

An example of this is substitution of metal-coated plastic components for solid metal components, such as those demonstrated by Ge *et al.* [4]. The *L*-band relativistic backward-wave oscillator (RBWO) of Ge *et al.* [4] featured a slow-wave structure (SWS) fabricated from a machined plastic base component, which was then layered with nickel and copper and then chromium to form a 100-μm metal coating. The metalized plastic SWS was found to perform comparably to a solid stainless steel SWS at power levels approaching 2 GW and pulse durations of 50 ns [4].

It is important to note that in linear beam tubes such as the aforementioned RBWO configuration, the SWS experiences high RF electric fields but would not be expected to experience substantial impacting current from the electron beam, and thus, it is not immediately evident if this technique can be extended to high-power crossed-field sources. In high-power crossed-field sources, such as relativistic magnetrons [1]–[3], [5], [6] and recirculating planar magnetrons (RPMs) [7]–[10], the SWS, which supports the high electric fields associated with the A–K gap bias as well as the RF wave, also serves as the anode for the electron beam and is directly impacted by a substantial fraction of the electron beam current [1]–[3], [5]–[10].

Herein, we investigate the possibility of using a metalized 3-D printed plastic anode structure in a relativistic RPM. We designed the printed anode structures as drop-in replacements (i.e., geometric duplicates) of the previously studied aluminum anode structures described by Franzi *et al.* [10]. Fabrication of two different 3-D printed anode structures, each metalized using a different process, is discussed. The RPM performance utilizing each of the printed anodes is compared with the recent performance results obtained using the solid aluminum anode structure as well as with the previous results [10].

II. Fabrication

The RPM-12a anode [Fig. 1(a)] is composed of two planar cavity arrays joined together by two recirculating bend sections. The four individual pieces are each machined conventionally from a block of aluminum and bolted together at the corners. The RPM-12b and c anodes were fabricated using a stereolithography (SLA) printing process, using DSM's Somos WaterShed XC 11122 photopolymer [11]. This process and polymer were chosen for their high resolution and dense construction, respectively. In previous work, the Air Force Research Laboratory has used this particular photopolymer successfully for high-voltage applications. The anodes were

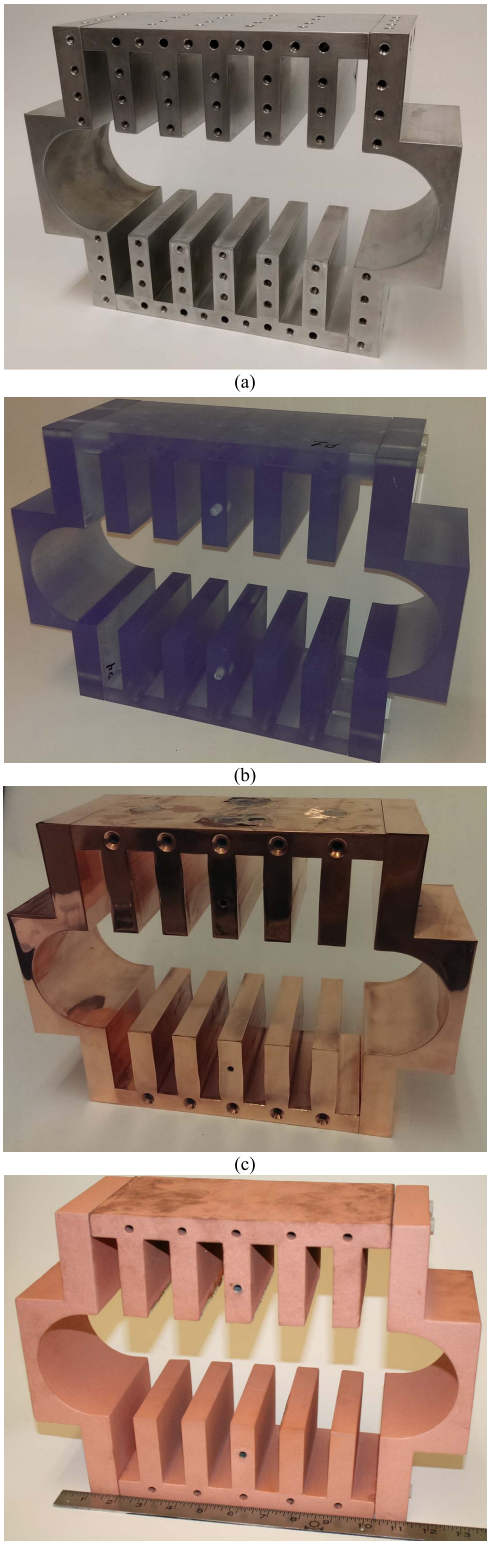

(a) (b) (c) (d)

Fig. 1. (a) RPM-12a anode, machined from aluminum, used as a baseline for comparison. (b) RPM-12b/c anode before coating process, composed of Water Shed XC 11122 photopolymer, which has properties to similar ABS or PBT. (c) RPM-12b anode, electroplated with copper. Some damage is visible on the top of the part, as a result of the coating process. (d) RPM-12c anode, coated via a copper thermal spray process. Discoloration on the top of the structure is a result of post-test handling without gloves.

each printed and coated as a four separate parts, each roughly 25 cm × 8 cm × 11 cm, and then assembly into the 34.2 cm wide anode shown in Fig. 1(b). Commercial SLA printers are

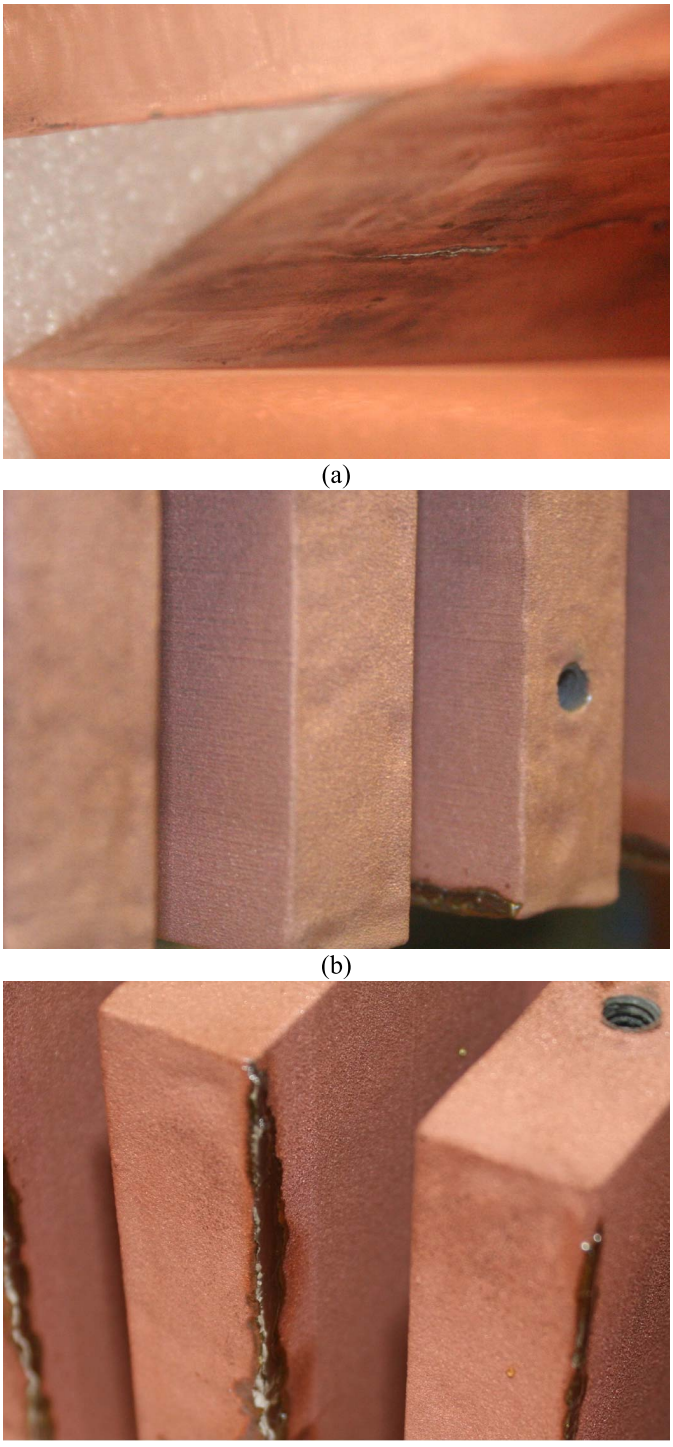

(a) (b) (c)

Fig. 2. Defects resulting from the fabrication process. (a) Nonuniform coating and thin cracks were present between the vanes of the electroplated structure. (b) Thermal spray process produced regions of uneven thickness, resulting in an orange peel-like appearance. (c) Thermal spray process also resulted in some cracks along vane edges, which we repaired with solder before testing.

capable of fabricating parts as large as 1 m^3, so the additively manufactured structure could have been fabricated as a single unit, but we chose to match the RPM-12a construction for direct performance comparison. The first set of pieces was coated by Fini-Finish [12] using a multistage process. The surface was first coated with a conductive epoxy and then electroplated with copper [Fig. 1(c)] to form RPM-12b. The

second set, RPM-12c, was thermal-sprayed with copper to create a conductive coating [Fig. 1(d)].

The RPM-12a anode, made of Al 6061, weighs 9.4 kg, whereas the uncoated plastic anode weighs 4.0 kg. The electroplated and thermally sprayed coatings add 1.09 and 1.24 kg to the structure, respectively. Measured at the anode vanes, we find the RPM-12b coating to be approximately 0.18-mm thick, whereas the RPM-12c coating is thicker at 0.23 mm. The higher surface roughness of the RPM-12c contributes somewhat to the thicker measurement.

A. Challenges and Defects

For these prototypes, there were some notable defects that resulted from the metallization processes. The electroplated structure (RPM-12b) did not have uniform coating thickness, particularly within the anode vanes. As can be seen in Fig. 1(c), the vanes widen slightly in the back of each cavity. Whereas the outer surfaces were relatively smooth, the interior of each cavity [Fig. 2(a)] did not coat evenly, leading to higher surface roughness and some surface discontinuities. The electroplated structure also suffered from delamination in several places. In these locations, a copper bubble would form, usually over 4 cm in diameter and $\sim$1 mm in height. We were initially concerned about trapped gas at the delamination sites and drilled small vent holes in many places to compensate, but many of the copper bubbles were between vanes and inaccessible. When placed under vacuum, the gas did not expand and damage the structure or create significant virtual leaks. In future work, the variation in coating thickness could be improved by careful design of the electroplating anodes, and delamination might be reduced with better surface preparation and alterations to the anode design to better accommodate the nuances of the electroplating process.

The thermal sprayed structure (RPM-12c) also suffered from variation in coating thickness [Fig. 2(b)]. As a line-of-sight process, thermal spray struggles to adequately and uniformly coat small holes or cavities, as well as sharp edges and corners. For the RPM-12c anode, the coating cracked in several places at the edge of the vanes [Fig. 2(c)] and had to be soldered to maintain electrical continuity.

III. Experimental Configuration

The Michigan electron long beam accelerator with a ceramic insulator stack (MELBA-C) was the driver for the RPM experiments, providing voltages between -250 and -300 kV for pulse lengths of 200 to 600 ns. A pair of pulsed electromagnets is positioned 21.6 cm apart in a pseudo-Helmholtz configuration and centered over the anode region to create a nearly uniform axial magnetic field, which was varied on a per-shot basis from 0.13 to 0.31 T. A #304 stainless steel vacuum chamber housed the magnetron and was operated at base vacuum pressures between 10^{-6} and 10^{-5} torr, as measured by an ion gauge mounted near the inlet to the cryopump, opposite to an SRS RGA-200 residual gas analyzer (RGA). A $CuSO_4$ resistive divider sampled the MELBA-C voltage pulse and a Rogowski coil within the vacuum chamber measured the current entering RPM-12a/b/c.

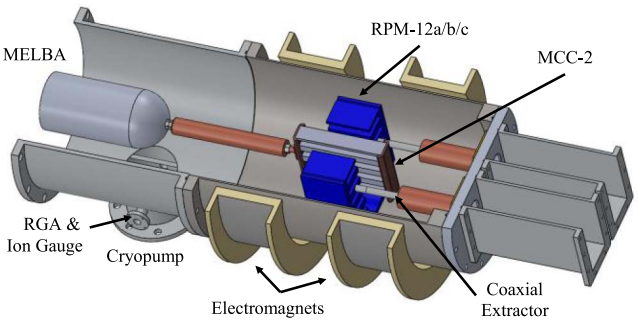

Fig. 3. Experimental configuration for RPM-12a, b, and c anode (blue) testing. Power is axially extracted via coaxial lines and launched into the waveguide by custom couplers. The center conductor of each coaxial line screws into the anode structure, making electrical contact at the surface.

Fig. 3 shows the experimental configuration used for RPM-12a/b/c, with a coaxial extraction system for calibrated power measurements. Microwave power was extracted via two symmetric coaxial waveguides with an inner conductor diameter of 0.75 cm and an outer conductor diameter of 2.5 cm, whose inner conductors were directly attached to the central vane of the anode structure under test. The coaxial transmission line entered a coax-to-waveguide coupler (DFA-650b) and was launched as a $TE_{1,0}$ mode in the waveguide, to be sampled by a directional coupler (-58 dB), and then dissipated in an Ecosorb load. The sampled microwave signals were transmitted to the Faraday cage using two RG-213U n-type cables (5 dB attenuation around 1 GHz) and attenuated by 22 dB using in-line attenuators. The signal was split using a 3-dB power divider to be: 1) directly sampled by a Tek7404 (5 GHz, 10 Gsamples/s per channel) oscilloscope to capture time-dependent frequency information and 2) rectified by calibrated Agilent 8472B low-barrier Schottky diode microwave detectors, which were connected to a Tek3054 oscilloscope for power measurement.

The cathode used for all tests was the mode control cathode 2 [13], which is composed of five hollow 1.9 cm $\times$ 3.8 cm rectangular tubes, resulting in an A–K gap of 2.6 cm. Including the end caps, it was 23 cm in length. To designate an emission region, 1.9-cm^2 velvet squares were attached to the center of the cathode using conductive silver epoxy, whereas the rest of the cathode was coated with several layers of Glyptal insulating paint.

Due to the axial extraction system, an endloss current measurement was not feasible. Endloss measurements were performed using a modification of the setup shown in Fig. 3, in which the axial extractors, waveguides, and chamber end plate were replaced by a stainless steel electron beam collection plate electrically isolated from the chamber by a 1-in Lexan ring. These measurements, in tandem with MAGIC simulations, were used to estimate the endloss current for shots conducted using the configuration shown in Fig. 3.

IV. Experimental Results

A. Magnetic Field Penetration

We compared the performance of the 3-D printed anodes with the baseline case of a four-piece aluminum anode,

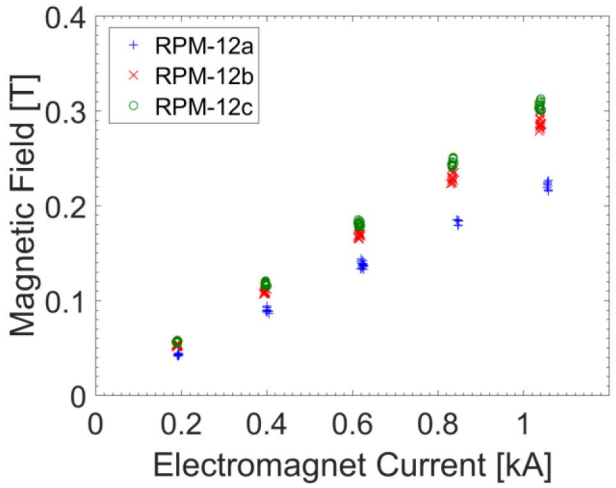

Fig. 4. Magnetic field at the center anode vane as a function of input current, measured at the start of voltage rise. The 3-D printed anodes result in substantially higher fields.

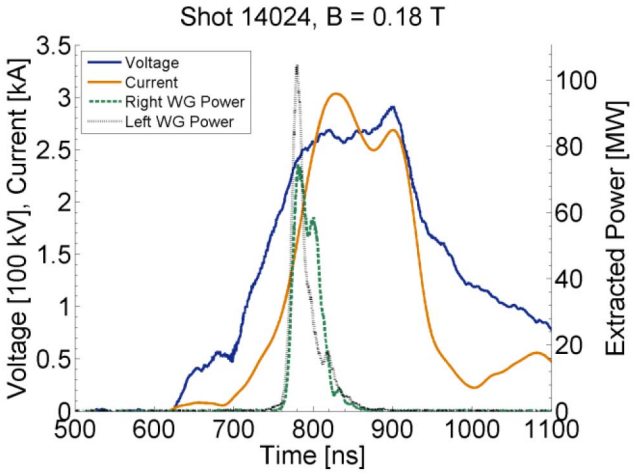

Fig. 5. Sample shot taken using RPM-12b. Microwave pulses were typically 50–100 ns in duration and occurred early in the voltage pulse. Current runaway at late times was well controlled for all the anodes tested.

TABLE I
DEVICE PERFORMANCE

	Average Peak Total Power [MW]	Average Peak Efficiency [%]
RPM-12a	101 +/- 19	20.0 +/- 6.5
RPM-12b	113 +/- 23	25.5 +/- 11.0
RPM-12c	91 +/- 21	28.7 +/- 9.1

In the range of axial magnetic fields from 0.15-0.22 T, the 3D printed anodes produced comparable power and efficiency to a traditionally fabricated anode. The uncertainties given are one standard deviation.

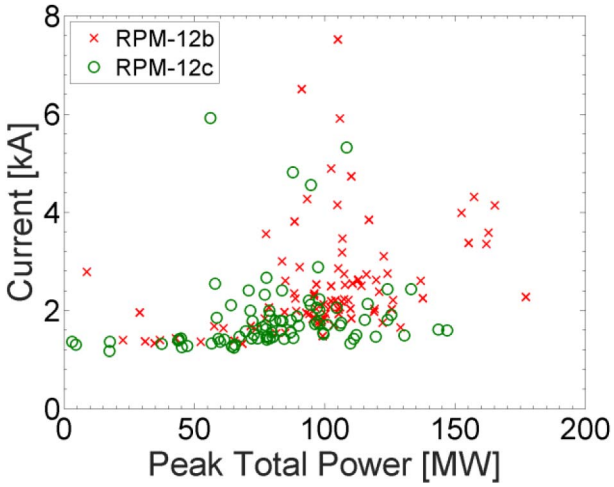

Fig. 6. 3-D printed anodes were subjected to substantial anode current and produced peak total power up to 170 MW without sustaining any observable damage or reduction in performance. It should be noted that this is the peak anode current, not the current at peak power.

RPM-12a. The differences in anode composition of the RPM-12b/c led to variation in magnetic field diffusion time relative to RPM-12a. As Fig. 4 shows, one of the advantages of using a metallized plastic structure, in conjunction with pulsed electromagnets, is an increase in peak field strength available within the magnetron. Consequently, for the same required magnetic field within the magnetron, a metallized plastic structure will have reduced requirements for its electromagnet. For our experimental setup, the electromagnets have a peak current of 1.1 kA, so the 3-D printed structures provided a broader parameter space to explore when identifying operating modes. In the future, it may be possible to create a more spatially uniform magnetic field within an RPM anode by adding and removing metallic material to optimize the field penetration in simulation. 3-D printed structures offer significant flexibility in this regard.

B. Microwave Performance

Our primary concern for the additively manufactured anodes was to verify that they could withstand repeated use in an HPM device and that their microwave performance was not adversely affected by their construction. Performance and durability characterization involved determination of operating modes and associated frequencies, peak power produced, efficiency of operation, and peak anode current experienced.

Fig. 5 shows the voltage, current, and power waveforms typically observed from the RPM. This particular example was produced by RPM-12b, but these waveforms were qualitatively very similar for all three anodes. Microwave pulses were approximately 50–100 ns in duration, with startup occurring early in the voltage pulse. The magnetic field for the 3-D printed anode was varied from 0.13 to 0.31 T, whereas the range of magnetic fields accessible to RPM-12a was limited to 0.15–0.22 T, as noted in the previous section.

As Table I shows, the power and efficiency of microwaves produced using the 3-D printed anodes was comparable to those of the solid metal RPM-12a. These data are also in line with previous tests of the RPM-12a [10]. The previous work did not use optimized magnetic field timing, leading to spatial variations in the magnetic field profile. Subsequent improvements in magnetic field uniformity motivated retaking the RPM-12a data. Averages and standard deviations are calculated using only data from shots with a magnetic field between 0.15 and 0.22 T. Applying that filter leaves approximately 45 shots in each data set. Peak total instantaneous efficiencies were determined using the total current (including

endloss). Specifically, the efficiency was determined by dividing the peak total output power (sum of both waveguides) by the product of current and voltage at the time of the peak total output power. Therefore, efficiencies in Table I are total efficiencies, not electronic efficiencies.

Performance characterization also involved identification of the operating frequencies, which could then be related to operating modes predicted from analytical theory and simulation. FFTs of the RF voltage traces revealed the magnetron primarily operated at approximately either 0.978 or 0.998 GHz. Based on simulations and theory, 0.978 GHz is the $5\pi/6$-mode and 0.998 GHz is the π-mode.

C. Durability

By varying the magnetic field, we were able to subject the anodes to a wide range of operating conditions, as shown in Fig. 6. As noted previously, the power extraction setup for the current RPM prototype does not allow a direct measurement of endloss current. Consequently, the range of anode currents shown in Fig. 6 is based on an estimate of 25% axial current loss (total, from each end of the cathode). For the purposes of this work, the precise value of current striking the anode is not essential. As Fig. 6 shows, the RPM-12b and c anodes were subjected to a peak anode current over 6 kA and produced a peak total power of over 150 MW without sustaining any observable damage or reducion in performance. A typical pulse experienced 2 kA of anode current and produced 100 MW of the total peak power. It should be noted that this is the peak anode current, not the current at peak power, and is not intended to relate the two quantities in any way. It simply shows the extent of the conditions these anode structures endured over the course of these tests. As a point of comparison, however, the total current at peak microwave power was between 1 and 4 kA for all anodes tested.

Both 3-D printed anodes were tested for over 100 shots, experiencing currents of up to 8 kA, peak microwave power generation up to 170 MW, and voltage pulses over -300 kV and 500 ns in duration. RPM-12b was visually inspected after 50 and 100 shots, with no discernable operationally induced damage. RPM-12c was inspected after 100 shots and also appeared completely unchanged. Upon conclusion of all 200 shots, it was evident that a small amount of copper had deposited back onto the cathode, as it had taken on a faint orange sheen. It should be noted that neither anode was subjected to any runaway current events, which typically induce notable damage on our solid aluminum anodes. More rigorous durability studies (1000s of shots and material analysis) are planned for future work.

Due to nonuniform electroplating, the surfaces of RPM-12b were not completely flat, leading to gaps where the anode and recirculating bend sections were bolted together [Fig. 7(a)]. These gaps caused poor electrical contact and minor arcing between the anode sections. Not all interfaces had visual evidence of arcing, and Fig. 7(b) shows the most prominent example. Future 3-D printed structures will need to consider this aspect of electroplating and either eliminate sections where electrical contact is a concern or install the appropriate RF gasket material.

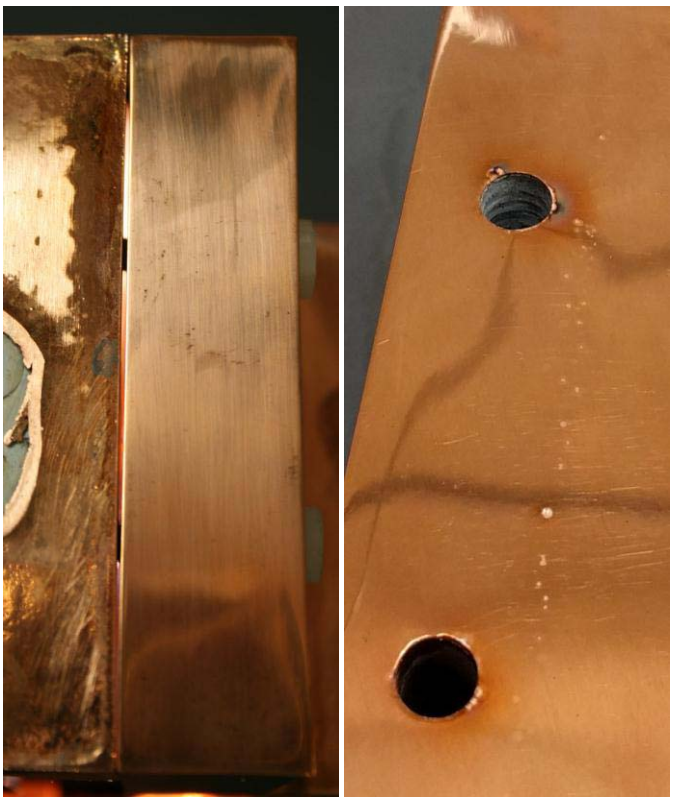

(a) (b)

Fig. 7. Uneven electroplating leading to (a) poor electrical contact at unions and (b) arcing between the parts during operation.

TABLE II
OUTGASSING COMPARISON

Pre-Shot Conditions	CO_2	CO	He	H_2	N_2	O_2	H_2O
RPM-12a	2	3	5	11	42	7	26
RPM-12b (1st day)	1	0	25	6	38	6	26
RPM-12b (2nd day)	1	0	35	4	35	5	20
RPM-12b (3rd day)	2	0	10	6	39	7	37
RPM-12c	2	3	5	11	44	8	27
Post-Shot Conditions							
RPM-12a	10	23	0	60	0	2	5
RPM-12b	11	25	0	60	0	0	4
RPM-12c	5	18	0	69	0	1	5

Gas inventories before each shot series primarily consisted of N_2 and H_2O, irrespective of the anode material. Post-shot outgassing was also similar for all three anodes; H_2 was the primary constituent, with CO, and CO_2, also consistently contributing.

No damage to the plastic substrate is expected, as the electrons should not penetrate either copper coatings. Assuming a 300-keV maximum energy when the electrons strike the anode (in reality, it will likely be much smaller, as the electrons give up some of their energy to the RF wave), the average path length traveled within copper, based on a continuous slowing down approximation, is 140 μm [14]. The average penetration distance along the angle of impact, however, is only 45 μm [15]. Even in the case of an optimal perpendicular impact at full beam energy, the electrons will not penetrate either copper coatings, whose thicknesses are over 200 μm.

D. Outgassing

Outgassing is one of the primary concerns for 3-D printed structures. For our experimental setup, the base vacuum chamber pressure was consistently at 9×10^{-6} torr, regardless

of which anode was in the chamber. For ultrahigh vacuum conditions, where a bakeout is required, the outgassing and robustness of the 3-D printed anodes would likely be more of a problem.

We first obtained a baseline measurement using RPM-12a, noting a preshot vacuum composition of primarily N_2 and H_2O, as shown in the top half of Table II. This is likely a result of a small vacuum leak at the microwave output windows. RPM-12b had similarly high N_2 and H_2O levels, but substantially higher He. This was a result of the chamber being under vacuum for a longer period before beginning the shot series. Fifteen shots were conducted the first day, the chamber was kept under vacuum, and 40 more shots were conducted the following day. As Table II shows, the He fraction continues to climb as high vacuum is maintained, eventually becoming the dominant component. In our system, this is likely the result of the higher He diffusion rate through rubber o-rings and its lower pumping speed within the cryopump, and possibly saturation of the charcoal arrays within the pump [16]. After the second day of testing RPM-12b, we opened the chamber to atmosphere to inspect the structure for any damage. No changes were observed and we finished the shot series the following day. Consequently, the He fraction decreased substantially. The chamber conditions before the third day are the most comparable to what was measured for the RPM-12a and c, as in all three cases, the chamber had been pumped by a cryopump for roughly 24 h. Comparing these three items in Table II, we see comparable initial conditions.

Beyond the passive outgassing, we used the RGA to investigate the gas released during each microwave pulse. This was accomplished by subtracting a background histogram taken immediately before the shot from the histogram taken immediately after the shot. We initially expected that we might see a signature gas for the 3-D printed structures, which would appear only in their histograms, or in a larger quantity, but the observed postshot outgassing was consistent for all three anodes, as shown in bottom half of Table II. As expected, the primary constituent was H_2, with CO and CO_2 also contributing significant fractions. Compared to the similar work in this area [17], [18], the relative fraction of water vapor was unusually low, possibly due to the lack of a fast gate valve. The H_2 fraction is likely slightly overestimated due to the way the RGA generates the histogram. We captured the histograms immediately after the shot, but the entire sweep from 1 to 50 amu still takes 1–2 s and starts at 1 amu. Consequently, the H_2 contribution is measured sooner, before the cryopump has reduced the inventory of all gases. Due to the small size of our chamber and the high pumping speed of the cryopump, the vacuum pressure rapidly decreases in the first 1–2 s. Attempts to reduce the pumping speed for better statistics resulted in unacceptably high base pressures, beyond what the RGA could reliably measure.

Due to the time required to complete a histogram sweep, we also monitored a single gas (CO_2) pressure as a function of time for all the three anodes (Fig. 8). The RGA can make this measurement at about 4 Hz, so we are able to more reliably

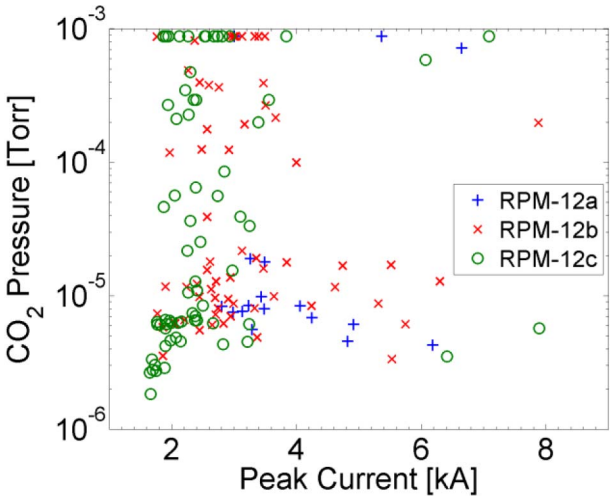

Fig. 8. Partial pressure of CO_2 within the chamber immediately following each shot, measured using the pressure versus time mode of the RGA at 4 Hz. All three anodes exhibited an average postshot peak pressure between 100 and 200 μtorr. The 3-D printed anodes had a larger percentage of high-pressure events, saturating the RGA at 8.5 $\times 10^{-4}$ torr.

capture the relative partial pressure of that gas. RPM-12a had an average postshot partial pressure of 1.48×10^{-4} torr, whereas RPM-12b and c averaged to 1.95×10^{-4} torr and 1.81×10^{-4} torr, respectively. As Fig. 8 shows, the majority of shots registered just under 1×10^{-4} torr for each anode, but the 3-D printed anodes had a larger percentage of high-pressure events, saturating the RGA at 8.5×10^{-4} torr. We speculate that these events were due to pockets of gas being released as the beam impacts the anode.

V. Conclusion

This paper demonstrates that additively manufactured materials have promising potential applications in high-power microwaves. Despite being subjected to highly energetic electron beams, the anodes displayed no visible damage and no deleterious effects on performance. By all indications in this limited study, they were acceptable replacements for a solid metal anode block, allowing the relativistic planar magnetron to produce microwave pulses in excess of 150 MW, comparable to the past results. Outgassing constituents from the additively manufactured structures were not substantially different from the aluminum control case, though they did exhibit slightly higher average postshot vacuum pressures. Furthermore, the plastic anodes exhibited a higher incidence of large increase in gas pressure during the microwave pulse. In these instances, the gas pressure briefly increased beyond what the RGA could reliably measure. For the film thickness and beam energies tested, electron penetration into the plastic structure is not a concern, with thermal effects expected to be the dominant damage mechanism. Given the short timescales and low repetition rate of this work, significant thermal effects were not encountered, but are an important component of continued work in this area. Similarly, whereas the 100 shots here demonstrate promising durability, a more exhaustive study is required to confidently predict material performance over thousands of pulses.

REFERENCES

[1] R. J. Barker, J. H. Booske, N. C. Luhmann, Jr., and G. S. Nusinovich, Eds., *Modern Microwave and Millimeter-Wave Power Electronics*. Hoboken, NJ, USA: Wiley, 2005.

[2] J. Benford, J. A. Swegle, and E. Schamiloglu, *High Power Microwaves*, 3rd ed. Boca Raton, FL, USA: CRC Press, 2016.

[3] J. C. Whitaker, *Power Vacuum Tubes Handbook*, 2nd ed. New York, NY, USA: CRC Press, 1999.

[4] X. Ge, J. Zhang, H. Zhong, and B. Qian, "A compact relativistic backward-wave oscillator with metallized plastic components," *Appl. Phys. Lett.*, vol. 105, no. 12, p. 123501, 2014.

[5] A. Palevsky and G. Bekefi, "Microwave emission from pulsed, relativistic *e*-beam diodes. II. The multiresonator magnetron," *Phys. Fluids*, vol. 22, no. 5, pp. 986–996, May 1979.

[6] M. R. Lopez *et al.*, "Relativistic magnetron driven by a microsecond e-beam accelerator with a ceramic insulator," *IEEE Trans. Plasma Sci.*, vol. 32, no. 3, pp. 1171–1180, Jun. 2004.

[7] R. M. Gilgenbach, Y. Y. Lau, D. M. French, B. W. Hoff, J. Luginsland, and M. Franzi, "Crossed field device," U.S. Patent 8 841 867 B2, Sep. 23, 2014.

[8] R. M. Gilgenbach, Y.-Y. Lau, D. M. French, B. W. Hoff, M. Franzi, and J. Luginsland, "Recirculating planar magnetrons for high-power high-frequency radiation generation," *IEEE Trans. Plasma Sci.*, vol. 39, no. 4, pp. 980–987, Apr. 2011.

[9] M. A. Franzi *et al.*, "Recirculating-planar-magnetron simulations and experiment," *IEEE Trans. Plasma Sci.*, vol. 41, no. 4, pp. 639–645, Apr. 2013.

[10] M. A. Franzi *et al.*, "Microwave power and phase measurements on a recirculating planar magnetron," *IEEE Trans. Plasma Sci.*, vol. 43, no. 5, pp. 1675–1682, May 2015.

[11] Dsm.com. (2016). *Somos WaterShed XC 11122: The Difference is Clear*, accessed on Jan. 3, 2016. [Online]. Available: http://www.dsm.com/products/somos/en_US/offerings/offerings-somos-water-shed.html

[12] Fini-Finish.com. (2016). *Fini Finish Metal Finishing | Chrome Plating | Rapid Prototype | Restoration*, accessed on Jan. 3, 2016. [Online]. Available: http://www.fini-finish.com/

[13] M. Franzi, R. Gilgenbach, Y. Y. Lau, B. Hoff, G. Greening, and P. Zhang, "Passive mode control in the recirculating planar magnetron," *Phys. Plasmas*, vol. 20, no. 3, p. 033108, 2013.

[14] M. J. Berger, J. S. Coursey, M. A. Zucker, and J. Chang. (2005). ESTAR, PSTAR, and ASTAR: Computer programs for calculating stopping-power and range tables for electrons, protons, and helium ions (version 1.2.3). National Institute of Standards and Technology, Gaithersburg, MD, USA, accessed on Jan. 8, 2016. [Online]. Available: http://physics.nist.gov/Star

[15] V. Lazurik, V. Moskvin, and T. Tabata, "Average depths of electron penetration: Use as characteristic depths of exposure," *IEEE Trans. Nucl. Sci.*, vol. 45, no. 3, pp. 626–631, Jun. 1998.

[16] D. M. Hoffman, B. Singh, and J. H. Thomas, III, *Handbook of Vacuum Science and Technology*. San Diego, CA, USA: Academic, 1998.

[17] M. E. Cuneo, "The effect of electrode contamination, cleaning and conditioning on high-energy pulsed-power device performance," *IEEE Trans. Dielectr. Electr. Insul.*, vol. 6, no. 4, pp. 469–485, Aug. 1999.

[18] R. M. Gilgenbach *et al.*, "Optical spectroscopy of plasma in high power microwave pulse shortening experiments driven by a μs *e*-beam," *IEEE Trans. Plasma Sci.*, vol. 26, no. 3, pp. 282–289, Jun. 1998.

Nicholas M. Jordan (S'05–M'13) received the B.S.E., M.S.E., and Ph.D. (plasma option) degrees in Nuclear Engineering and Radiological Science from the University of Michigan (UM), Ann Arbor, MI, USA, in 2002, 2004, and 2008, respectively.

He was an Assistant Research Scientist with the Plasma, Pulsed Power, and Microwave Laboratory, UM, in 2013. He was with Cybernet Systems, Ann Arbor, where he was involved in microwave vehicle stopping technology for five years. His current research interests include high-power microwave devices, pulsed power, laser ablation, Z-pinch physics, and plasma discharges.

Geoffrey B. Greening (S'12) received the B.S.E. and M.S.E. degrees in nuclear engineering and radiological sciences (plasma option) from the University of Michigan (UM), Ann Arbor, MI, USA, in 2010 and 2012, respectively, where he is currently pursuing the Ph.D. degree.

He has been with the Safeguards Laboratory, Oak Ridge National Laboratory, Oak Ridge, TN, USA, L-3 Communications Electron Devices, Williamsport, PA, USA, and the Directed Energy Directorate, Air Force Research Laboratory, Kirtland Air Force Base, Albuquerque, NM, USA. He is currently a Graduate Student Research Assistant with the Plasma, Pulsed Power, and Microwave Laboratory, UM, under the supervision of Prof. R. M. Gilgenbach. His current research interests include high power microwave source development.

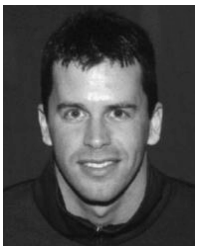

Brad W. Hoff (S'04–M'10) received the B.S. degree in physics from the U.S. Naval Academy, Annapolis, MD, USA, in 1999, and the M.S.E. degree in nuclear engineering, the M.S.E. degree in electrical engineering, and the Ph.D. degree in nuclear engineering from the University of Michigan, Ann Arbor, MI, USA, in 2006, 2007, and 2009, respectively.

He is currently a Research Physicist with the Directed Energy Directorate, Air Force Research Laboratory, Kirtland Air Force Base, Albuquerque, NM, USA. His current research interests include high-power microwave sources and directed energy technology.

Sabrina S. Maestas was born in NM, USA, in 1984. She received the B.S. degree in mechanical engineering from the University of New Mexico, Albuquerque, NM, USA, in 2008.

She is currently a Mechanical Engineer with the Directed Energy Directorate, Air Force Research Laboratory, Kirtland Air Force Base, Albuquerque, NM, USA.

Steven C. Exelby, (S'15) photograph and biography not available at the time of publication.

Ronald M. Gilgenbach (LF'06) received the B.S. and M.S. degrees from the University of Wisconsin, Madison, WI, USA, in 1972 and 1973, respectively, and the Ph.D. degree in electrical engineering from Columbia University, New York, NY, USA, in 1978.

He spent several years as a member of the Technical Staff with Bell Labs, Murray Hill, NJ, USA, in the 1970s. From 1978 to 1980, he performed gyrotron research with the Naval Research Laboratory (NRL), Washington, DC, USA, and performed the first electron cyclotron heating experiments on tokamak plasma with the Oak Ridge National Laboratory, Oak Ridge, TN, USA. He joined as a Faculty Member with the University of Michigan (UM), Ann Arbor, MI, USA, in 1980, where he became the Director of the Plasma, Pulsed Power and Microwave Laboratory. He has supervised 46 graduated Ph.D. students with UM. He is currently a Chair and a Chihiro Kikuchi Collegiate Professor with the Nuclear Engineering and Radiological Sciences Department, UM. He has authored over 165 articles in refereed journals and books, and has five patents granted. He has collaborated in research with scientists with the Air Force Research Laboratory, Wright-Patterson Air Force Base, OH, USA, Sandia National Labs, Albuquerque, NM, USA, NASA Glenn, Cleveland, OH, USA, Northrop-Grumman, Falls Church, VA, USA, L-3 Communications, New York, NY, USA, General Motors Research Labs, Detroit, MI, USA, the Los Alamos National Laboratory, Los Alamos, NM, USA, Fermilab, Batavia, IL, USA, Naval Research Laboratory, and the Institute of High Current Electronics, Tomsk, Russia.

Dr. Gilgenbach is a fellow of the American Physical Society Division of Plasma Physics. He received the NSF Presidential Young Investigator Award in 1984, and the 1997 Plasma Sciences and Applications Committee (PSAC) Award from the IEEE. He served as a PSAC Chair in 2007 and 2008. He was an Associate Editor of the *Physics of Plasmas* journal.